Membrane-Protein Binding Measured with Solution-Phase Plasmonic Nanocube Sensors

Hung-Jen Wu[1, 2, 3], Joel Henzie[2], Wan-Chen Lin[1,2], Christopher Rhodes[1,2,4], Zhu Li[5], Elodie Sartorel[5], Jeremy Thorner[5], Peidong Yang[2], Jay. T. Groves[1,2, 3, 6]*

[1] Howard Hughes Medical Institute, University of California, Berkeley, California, USA

[2] Department of Chemistry, University of California, Berkeley CA USA

[3] Physical Biosciences Divisions, Lawrence Berkeley National Laboratory, Berkeley CA USA

[4] Department of Mechanical Engineering, University of California, Berkeley CA USA

[5] Department of Molecular and Cell Biology, Division of Biochemistry, Biophysics and Molecular Biology, University of California, Berkeley, California, USA

[6] Materials Sciences Divisions, Lawrence Berkeley National Laboratory, Berkeley CA USA

* To whom correspondence should be addressed jtgroves@lbl.gov

Abstract

We describe a solution-phase sensor of lipid-protein binding based on localized surface plasmon resonance (LSPR) of silver nanocubes. When silica-coated nanocubes are mixed into a suspension of lipid vesicles, supported membranes spontaneously assemble on their surfaces. Using a standard laboratory spectrophotometer, we calibrate the LSPR peak shift due to protein binding to the membrane surface and then characterize the lipid-binding specificity of a pleckstrin-homology domain protein.

Introduction

The intracellular environment is dominated by membrane surfaces, and a significant fraction of biochemical processes involves membranes[1]. Analytical methods for membrane analysis based on chemical labeling have many drawbacks, and hence there is substantial demand for quantitative label-free detection. Techniques, such as backscattering interferometry[2], colloidal assembly[3], nanowire arrays[4], microcantilevers[5], acoustic sensing[6], and surface plasmon resonance[7] have all been reported, but most are impractical for widespread adoption in biological laboratories. More promising for protein-lipid interactions is localized surface plasmon resonances (LSPR), in which binding causes measurable changes in refractive index[8-11]. However, conventional LSPR techniques typically rely on analyte capture onto nanofabricated surfaces and often necessitate sophisticated instrumentation. The need for quantitative label-free detection methods that are simple, robustly reproducible, and accessible to scientists using generic laboratory equipment remains unmet.

Here, we report a platform that enables label-free measurements of protein binding to membrane surfaces on a standard laboratory spectrophotometer. We have previously described label-free detection using the LSPR of thiolated silver nanocubes immobilization on flat substrates.[9] This configuration required multiple reactions, a customized detection system, and ultimately proved similarly impractical as the other methods mentioned above. A substantial improvement in utility is achieved here by modifying the system to allow measurements to be performed entirely in the solution phase. Highly monodisperse Ag nanocubes were prepared by an established synthetic protocol[12] (**Supplementary Fig.1**). In order to create a favorable surface for membrane assembly and suspension in solution, an ultra-thin layer of silica was then grown using Stöber synthesis (Methods). Transmission electron microscopy (TEM) micrographs revealed a uniform silica shell covering the Ag surface with average thickness 3.9 ± 0.2 nm (n = 5, mean ± s.d.) and corners with curvature radius of 19 nm (**Fig.1a** and **1b**). Elemental maps acquired by high-angle annular dark field scanning TEM show that the silicon and oxygen intensities were strongest on the edges of Ag@SiO_2 core-shell nanocube particles (silver core @ silica shell), indicating the shell is conformal and uniform (**Fig.1c-1f**, and **Supplementary Fig.2**). Additionally, the SiO_2 coating provides a shelf life in excess of one year by slowing silver oxidation.

Ag@SiO_2 nanocubes exhibit a sharp quadrupolar LSPR scattering peak (**Fig.1g**). This is easily observed in the extinction spectrum of a suspension of nanocubes using standard laboratory tools such as a transmission ultraviolet-visible (UV-vis) spectrophotometer, micro-volume spectrometer (*e.g.* NanoDrop), dark-field microscopy (**Supplementary Fig.3**), or light scattering spectrophotometer (**Supplementary Fig.4**). Electromagnetic simulations based on the actual particle geometry confirm the time-averaged electric field norms exhibit quadrupole resonance with the highest near-field enhancement near the nanocube corners (**Fig.1h**). At quadrupole resonance, $|E|/E_0$ decays to 50% of its value at the silica-media interface over about 10 nm distance. The silica layer is sufficiently thin that the LSPR field still penetrates a lipid bilayer of 3-5 nm thickness (**Supplementary Fig.5**). A widely used figure of merit (FOM) for LSPR is the peak shift per refractive index unit (nm / RIU) normalized to the linewidth of the LSPR peak (details in Method section). The FOM for Ag@SiO_2 nanocubes is 1.7 versus 2.4 for bare silver nanocubes.

Supported lipid bilayers form spontaneously upon mixing Ag@SiO_2 nanocubes into a lipid vesicle suspension (**Fig.1g**). Supported membrane formation was confirmed using fluorescence recovery after photobleaching (FRAP) experiments to test the lateral fluidity and connectivity of membranes covering substrate-adsorbed nanocubes[9](**Supplementary Fig.6**). The nanocubes were first immobilized on planar glass substrates and then exposed to lipid vesicle suspensions so that a supported lipid bilayer formed on top of both the glass substrate and nanocubes. Bilayers on Ag@SiO_2 nanocube-covered substrates exhibited almost identical recovery behavior to bilayers on bare glass (**Supplementary Fig.6**). This result indicates that the supported bilayers on Ag@SiO_2 nanocubes are fluid and connected to the bilayer on surrounding glass. The magnitude of fluorescence recovery also confirms that the majority of nanocubes are covered with lipid membrane[9]. In contrast, bilayers on a bare Ag nanocube-covered substrates exhibited similar recovery times but only 60% of the recovery on bare glass, which illustrates that lipids absorbed on bare nanocubes did not form a fluid and continuous bilayer with the surrounding fluid bilayer. Although it has been suggested that supported lipid bilayer cannot form on a highly curved surfaces (11 nm radius of curvature) due to high elastic energy [13], we did not observe any such limitation on the Ag@SiO2 nanocubes (19 nm radius of curvature over corner).

The LSPR response of the system is calibrated by monitoring the essentially irreversible binding of streptavidin to biotinylated lipids in the nanocube supported membrane (**Supplementary Fig.7**). We employed three different approaches to control the surface density of membrane-bound streptavidin: (i) titrating biotinyl-cap-PE in bilayer; (ii) titrating streptavidin in solution; and (iii) measuring unbound fluorescent streptavidin (details in Supplementary Discussion). LSPR shifts were measured at different known surface densities of streptavidin and exhibited a linear relation with protein density (**Fig.2a**). Consistent LSPR responses of 0.191 ± 0.025 ng mm^{-2} nm^{-1} (n = 3, mean ± s.d.) were determined by three independent approaches (**Supplementary Table 1**).

To assess that bilayer-coated Ag@SiO_2 nanocubes can quantify protein binding accurately, we compared the system with the established method of multi-component fluorescence correlation spectroscopy (multi-component FCS)[14]. Cholera toxin subunit B (CTB) binding to the membrane-associated receptor G_{M1} was used as a model system (**Fig.2b**). In multi-component FCS measurements, lipid vesicles and CTB were labeled with different fluorophores and the concentrations of bound and unbound CTB were monitored. The average size of vesicles was determined independently by dynamic light scattering, which allowed determination of the surface density of vesicle-bound CTB (details in Supplementary discussion). Using the same materials and under the same experimental conditions, nanocube measurements were performed independently. LSPR response was converted to protein surface density using the LSPR response to protein mass change measured in the biotin-streptavidin system, 0.191 ng mm^{-2} nm^{-1} (**Supplementary table 1**). Kinetics measured by multi-component FCS and nanocube methods reached equilibrium state and the same surface density after 1000 sec (**Fig.2b**). It is worth noting that unlike FCS, which only works at low concentration, the nanocube detection strategy has a much broader working range. (details in Supplementary Discussion)

Finally, we used the Ag@SiO_2 nanocube assay to examine the heretofore unknown lipid binding specificity of a prototypic mitogen-activated protein kinase (MAPK) scaffold protein,

Ste5. Ste5 contains a pleckstrin-homology domain (PH domain, residues 388-518) that is essential for its membrane recruitment and function, but the dependence of Ste5 binding on membrane composition is not well known[15]. We investigated the binding of Ste5 to membranes with and without $PI(4,5)P_2$. GST-Ste5 PH domain fusion proteins (corresponding to Ste5 residue 369-517), with and without R407S and K411S mutations thought to abrogate lipid binding, were constructed, expressed, and purified from *Entamoeba coli*. To avoid interference of detergent with the membrane assay, we eliminated its use during protein purification (Supplementary discussion). Only wildtype GST-Ste5 PH domain bound to the membrane surface (**Fig2c**). Although more Ste5 binding was observed on $PI(4,5)P_2$ membranes, appreciable binding was also observed on membranes without $PI(4,5)P_2$. This may be due to the presence of phosphatidic acid lipids, which have been observed to association with PH domains in other protein systems[16]. Binding curves were established to compute the binding affinity of GST-Ste5 on different compositions of membranes (**Fig.2d**). At similar lipid compositions, we have previously reported rough estimates of K_d for Ste5-membrane binding using filter-immobilized lipids, liposome flotation assays, and surface plasmon resonance (SPR), that suggest a dissociation constant in the 5-10 μM range[15]. However, the lipid immobilization and tethering required for the filter and SPR assays are strongly disruptive of the membrane surface environment[7] and liposome flotation assays are intrinsically error-prone. Thus, among all of the measurements, we consider the nanocube assay to be the most consistent and most accurate.

We report a core-shell $Ag@SiO_2$ nanocube sensor that can measure protein binding to its membrane-coated surfaces. No complicated fabrication is necessary and these sensors can be prepared on the gram scale (> 10^{14}) at minimal cost. Solution phase measurements readily integrate 10^{12} nanocubes in the illumination area of a standard spectrophotometer cuvette. This provides sensitivity of approximately 0.19 ng cm^{-2} based on 0.01nm standard error of 20 consecutive LSPR measurements (details in Supplementary discussion), in contrast to the immobilized format[9] (10^9 nanocubes; sensitivity = 1.5 ng cm^{-2}). This method is applicable to analytes that bind lipid membranes or membrane proteins, including proteins, peptides, nucleic acids, or even entire cells. The biggest advantage of this method is that simply adding $Ag@SiO_2$ nanocubes to a vesicle suspension produces a system in which analytes binding to the membrane surface can be read out by standard spectral technique widely available in most labs, without labeling.

Acknowledgments

This work was supported by the Director, Office of Science, Office of Basic Energy Sciences, of the US Department of Energy under contract no. DE-AC02-05CH11231 (to J.T.G.) and by US National Institutes of Health Research Grant GM21841 (to J.T.). P.Y. would like to acknowledge the support from King Abdulaziz University.

Author Contributions

H.-J.W. and J.T.G. conceived the solution-phase nanocube sensor strategy. H.-J.W. implemented the experiments, J.H. synthesized nanocubes and performed TEM, W.-C.L. performed FCS measurements, C.R. performed LSPR simulations and Z.L. and E.S. prepared Ste5 proteins. H.-J.W., C.R. and J.T.G. wrote the manuscript. J.T.G., J.T. and P.Y. supervised the project. All authors discussed the results and commented on the manuscript at all stages.

Competing Financial Interests

The authors declare no competing financial interests.

Figure legend

Figure 1. The physical properties of Ag@SiO_2 core-shell nanocube. (**a**) & (**b**) TEM images of Ag@SiO_2 nanocube. (**a**) is the close-up image of figure (**b**). (**c**)~(**f**) The elemental maps obtained by high-angle annular dark field scanning TEM (HAADF-STEM) with energy dispersive x-ray spectroscopy (EDS). (**c**) to (**f**) represent silver, silicon, oxygen, and carbon, respectively. (**g**) Top: Detection procedure of nanocube sensors. Supported lipid bilayers are formed by vesicle fusion onto the silica surface, and protein binding is monitored by shifts in the LSPR extinction spectrum. Bottom: Typical spectra of membrane coverage and protein binding to the membrane surfaces. Sequential addition of lipid vesicles, BSA, and streptavidin causes LSPR red shifts. (**h**) Electric field norm ($|E|/E_0$) in decibel (dB) of a nanocube at resonance (n = 1.33303, λ_0 = 474 nm) computed using finite-element analysis.

Figure 2. Calibration of the nanocube assay. (**a**) Relation between LSPR shift and number of streptavidin per nanocube (left vertical axis) and surface density (right axis) measured by titration of biotinyl-cap-PE, titration of streptavidin, and fluorescence measurement of streptavidin concentration. Linear fit slopes are reported in Supplementary Table 1. (**b**) Top: Concentrations of bound and unbound CTB are detected by multi-component FCS. Alexa 594-CTB binds to vesicles (average diameter 120 nm) containing 0.5% G_{M1} and 0.5% BODIPY-FL-DHPE lipids. BODIPY-FL-DHPE was used to determine the average number of vesicles diffusing within the excitation spot. Bottom: Binding kinetics measured by multi-component FCS and nanocube assay. (Error bar of FCS, n=20, mean ± s.d.) CTB surface density was respectively calculated from known vesicle size and LSPR response to protein mass change in streptavidin-biotin systems (0.191 ng mm^{-2} nm^{-1}). (**c**) Binding kinetics of wild-type and R407S K411S mutant of GST-Ste5 PH to different membrane surfaces. Concentrations of GST-Ste5 PH= 1.6 μM; GST-Ste5 PH mutant = 1.6 μM) (**d**) Equilibrium binding curves of GST-Ste5 PH to bilayers K_d = 0.49 ± 0.33 μM (PI(4,5)P_2 bilayer) and 1.6 ± 0.45 μM (PI(4,5)P_2-free bilayer) (n=3, mean ± s.e.m.) Error limits of K_d are derived from the statistical error of curve fitting.

Methods

Materials

Lipids. The following lipids were purchased from Avanti Polar Lipids (Alabaster, AL): 1,2-dioleoyl-sn-glycero-3-phosphocholine (DOPC), 1,2-dioleoyl-sn-glycero-3-phosphoethanolamine-N-(cap-biotinyl) (Biotinyl-Cap-PE), Ganglioside G_{M1} (G_{M1}), 1,2-dioleoyl-sn-glycero-3-phospho-L-serine (DOPS), 1,2-dioleoyl-sn-glycero-3-phosphate (DOPA), 1,2-dioleoyl-sn-glycero-3-phosphoethanolamine (DOPE), L-α-phosphatidylinositol (PI), and L-α-phosphatidylinositol-4,5-bisphosphate ($PI(4,5)P_2$). The fluorescent lipid probes, Texas Red 1,2-dipalmitoyl-sn- glycero-3- phosphoethanolamine (Texas red DPPE) and N-(4,4-difluoro-5,7-dimethyl-4-bora-3a,4a-diaza-s-indacene-3-propionyl)-1,2-dihexadecanoyl-sn-glycero-3-phosphoethanolamine, triethylammonium salt (BODIPY-FL-DHPE), were purchased from Invitrogen .

Ethanol (200 proof), tetraethyl orthosilicate (TEOS), 28% ammonium hydroxide solution, unlabeled recombinant streptavidin, and bovine serum albumin were purchased from Sigma-Aldrich. The fluorescent proteins Alexa Fluor 647 streptavidin and cholera toxin subunit B (CTB) Alexa Fluor 594 were purchased from Invitrogen. Streptavidin and CTB binding experiments were performed in 1× PBS buffer (Mediatech). GST-Ste5 binding measurements were performed in HKME buffer (20 mM HEPES-KOH at pH = 7.0, 160 mM KOAc, 1 mM $MgCl_2$, 0.1 mM EGTA).

Silica-coated nanocube

Ag nanocubes are synthesized using the polyol method[12, 17, 18] capped with poly(vinylpyrrolidone) (PVP), and stored in ethylene glycol before use. Silica shells were coated on Ag nanocubes using Stöber process.[19] The concentration of ammonium hydroxide and reaction time affected the thickness and quality of the silica layer.[20] Ag nanocubes were first washed extensively with ethanol. Silica layers were coated by mixing 7.5ml of Ag nanocube suspension in ethanol with 1950 μl of water, 600 μl of TEOS, and 300 μl of 0.28% ammonium hydroxide. The solution was sonicated during the entire reaction. After 40min reaction, the $Ag@SiO_2$ nanocubes were washed with ethanol to remove the reagents and then washed extensively with water. The $Ag@SiO_2$ nanocubes were stored in deionized water for future use.

LSPR measurement

Various approaches have been reported to collect nanoparticle extinction spectra[21]. We employed a general transmission ultraviolet-visible (UV-vis) spectrophotometer (Cary 100, Varian). Typically, spectral shifts were monitored by detecting the prominent quadrupolar LSPR peak λ_{max}. These peaks were determined by fitting transmission spectra to a seventh-order polynomial (**Fig. 1g**). The dependence of LSPR peak shift on refractive index was measured in water-glycerol solutions of various ratios. To explore the effect of the silica shell, the refractive index sensitivity of $Ag@SiO_2$ nanocubes was compared to Ag nanocubes using solutions of water and glycerol. (**Supplementary Fig.8**) LSPR sensitivity was quantified using the widely reported figure of merit (FOM) calculated by dividing refractive index sensitivity by the line width of resonance spectrum (FOM = $S/\Delta\lambda$)[22, 23] The refractive index sensitivity (S) was evaluated from **Supplementary Fig.8** and represented as peak shift (reported in nm or eV) per refractive index unit (RIU). The line width of the resonance spectrum ($\Delta\lambda$) was obtained from

the full width at half maximum (FWHM) of the LSPR peak (**Fig. 1g**).

To demonstrate the applicability of other detection schemes, scattering spectra were also measured by (1) dark field scattering microscopy using a dark field condenser and spectrometer (USB2000, Ocean Optics), and (2) a fluorescence spectrophotometer (Varian, Inc) configured for 90 degree scattering detection.

The nanocube concentrations were determined by counting deposited nanocubes on glass substrates. The silica-coated nanocube solutions were incubated in a sedimentation chamber for two days to create monolayers of nanocubes. Dark field microscopy was used to observe the nanocubes deposited on the bottom of each sedimentation chamber. A homemade image analysis program was developed to count the number of nanocubes in each imaging frame.

Bilayer preparation

Lipid vesicles. The desired composition of lipids was first mixed in chloroform. The mixture was then dried in a round bottom flask followed by desiccation under nitrogen for at least 30 minutes. Lipid films were then hydrated with 18.2 MΩ·cm deionized (DI) water. The resulting suspension was probe sonicated to clarity in an ice bath and ultracentrifuged at 4 °C for 45 min. The top small unilamellar vesicle (SUV) solution was extracted for use in experiments. For FCS and GST-Ste5 binding experiments, SUVs were prepared through an extrusion process. Instead of sonicating, the hydrated lipids were extruded through 100 nm polycarbonate pore filters (Whatman, UK) until the suspension reached clarity. The vesicle used in FCS measurement contains 0.5% G_{M1}, 0.5% BODIPY-FL-DHPE and 99% DOPC lipids. The lipid membranes used in GST-Ste5 PH binding experiment contain: (1) 53% DOPC, 22% DOPE, 10% DOPS, 5% DOPA, 10% PI for PIP_2-free bilayer and (2) 53% DOPC, 22% DOPE, 10% DOPS, 5% DOPA, 5% PI, 5% $PI(4,5)P_2$ for PIP_2 bilayer.

Supported lipid bilayers. Supported lipid bilayers were formed by adapting a standard vesicle fusion technique[3]. Bilayers were assembled by combining equal volumes of SUV suspension and the desired buffer in a small centrifuge tube, followed by vortex mixing. Excess vesicles and salt were removed by rinsing twice with the buffer using a benchtop centrifuge (minicentrifuge, VWR, maximum RCF = 2000 g). Membrane-coated particles were then diluted to the desired working concentration and introduced into the spectrophotometer cell.

Protein binding measurement

Bilayer-coated nanocubes were incubated with 0.05 mg ml^{-1} BSA solution to block non-specific binding prior to adding desired proteins. Fifteen consecutive scans were performed to obtain the average λ_{max} of the LSPR quadrupolar peak as a baseline. The desired amount of protein was directly cast into the spectrophotometer cell (400 μL sample volume) followed by pulse vortexing of the mixture. Spectra in the range of 430 nm to 480 nm were scanned immediately after mixing at 0.5 nm spectral resolution. The maximum attainable scanning rate was six seconds per spectrum, limited by the configuration of the UV-vis spectrophotometer. To minimize the use of protein in GST-Ste5 binding experiments, these measurements were performed with a sub-microvolume optical cuvette. Different volumes of protein (0.5-15μl) were incubated with 20μl of bilayer-coated $Ag@SiO_2$ nanocube sensors for two hours. The average λ_{max} of the LSPR quadrupolar peak were obtained from ten consecutive spectra. All experiments were performed at room temperature.

Fluorescent correlation spectroscopy

Fluorescence correlation spectroscopy (FCS) measurements were performed on a home-built FCS apparatus based on a Nikon TE2000 inverted fluorescence microscope as described previously[24]. Two laser beams, 488 nm and 568 nm, were coupled into an optical fiber and focused by a 100× TIRF objective (Nikon) onto the sample to excite the fluorescent probes. The emitted light was filtered through notch filters and a confocal pinhole then separated by a 560 nm long-pass filter. Before focusing onto two avalanche photodiodes (APDs) (Perkin and Elmer), two color filters were used to minimize spectrum crosstalk. The photon arrival time was recorded and the auto-correlation functions of the two APD signals were calculated with a hardware correlator (Correlator.com) in real time. Using a double-labeled supported lipid bilayer as a sample, overlapping detection volumes were obtained by careful alignment of a collimator lens after the optical fiber and fine adjustment of the objective lens correction collar[25]. Measurements were made in eight-well chambered coverglass (Nunc) that were first soaked with 0.1 M NaOH for 20 min to clean the bottom surface. The supported lipid bilayers (100% DOPC) were formed on the bottom surface by vesicle fusion. The chamber was incubated with 0.1mg/ml BSA to prevent the protein and vesicle absorption. The size and the structure factor *s* of the excitation volume were calibrated using 200nM fluorescein in 1M NaOH solution with a known diffusion coefficient (D = 300 μm^2 s^{-1})[26]. All other measurements were performed at 24.5 °C in 1× PBS buffer.

The model system, CTB binding to vesicles containing the membrane associated receptor monosialoganglioside G_{M1}, was selected to directly compare FCS and nanocube measurements. To obtain a narrow size distribution of vesicles, SUVs were prepared by the standard extrusion method described above. Vesicles of 120 nm average diameter containing 0.5% G_{M1}, 0.5% BODIPY-FL-DHPE and 99% DOPC lipids were measured by dynamic light scattering (Brookhaven Instruments Corp.). A detailed description of the multi-component FCS calculations is shown in the Supplementary Discussion.

TEM

Ag@SiO_2 nanocubes were imaged using high-resolution transmission electron microscopy (JEOL 2100-F, 200 kV). The elemental x-ray analysis maps were generated using high-angle annular dark field scanning TEM (HAADF-STEM) with an energy dispersive x-ray spectroscopy (EDS) detector. TEM images revealed nanocube a lateral dimension of 98 nm, 19 nm radius of curvature at the edges, and silica shell thickness of 3.9 nm.

LSPR simulation

Finite element simulations using COMSOL were used to model the LSPR of silica-coated silver nanocubes. Free tetrahedral meshing of the geometry observed in TEM was performed in COMSOL, and further refined in the vicinity of the silica shell. The final mesh contained 359,000 tetrahedral elements, and convergence of absorption spectra within 0.1% error was confirmed by comparing results from a coarser mesh.

Frequency-domain scattered electric field solutions were computed using COMSOL's RF module for a background oscillating field of arbitrary amplitude 1 V m^{-1}. Real and imaginary refractive index dispersion was interpolated from literature tables for silver and silica [27]. The nanocube was simulated inside a sphere of diameter 400 nm, sufficiently large for all near-field effects to be negligible at the system boundary. A perfectly matched layer (PML) was

additionally incorporated to cancel any reflection artifacts in the simulation. Field solutions were calculated for 50-100 different frequencies at a time.

GST-Ste5 Protein preparation

GST-Ste5 PH domain fusion proteins with and without R407S K411S mutations (corresponding to Ste5 residue 369-517) were constructed, expressed, and purified from *Escherichia coli* as described by Garrenton et al [15]. The use of Tween-20 detergent was omitted during protein purification to avoid the influence of detergent on lipid bilayers. Prior to binding experiments, GST-Ste5 proteins were treated with Amicon centrifuge filters (Millipore) for further purification and buffer exchange.

Reference

1. Kuriyan, J. & Groves, J.T. *Nat. Struct. Mol. Biol.* **17**, 659-665 (2010).

2. Baksh, M.M., Kussrow, A.K., Mileni, M., Finn, M.G. & Bornhop, D.J. *Nat. Biotechnol.* **29**, 357-U173 (2011).

3. Baksh, M.M., Jaros, M. & Groves, J.T. *Nature* **427**, 139-141 (2004).

4. Zheng, G.F., Patolsky, F., Cui, Y., Wang, W.U. & Lieber, C.M. *Nat. Biotechnol.* **23**, 1294-1301 (2005).

5. Braun, T. et al. *Nat. Nanotechnol.* **4**, 179-185 (2009).

6. Cooper, M.A. *J. Mol. Recognit.* **17**, 286-315 (2004).

7. Beseničar, M., Maček, P., Lakey, J.H. & Anderluh, G. *Chem. Phys. Lipids* **141**, 169-178 (2006).

8. Dahlin, A. et al. *J. Am. Chem. Soc.* **127**, 5043-5048 (2005).

9. Galush, W.J. et al. *Nano Lett.* **9**, 2077-2082 (2009).

10. Jonsson, M.P., Jonsson, P., Dahlin, A.B. & Hook, F. *Nano Lett.* **7**, 3462-3468 (2007).

11. Baciu, C.L., Becker, J., Janshoff, A. & Sonnichsen, C. *Nano Lett.* **8**, 1724-1728 (2008).

12. Tao, A., Sinsermsuksakul, P. & Yang, P.D. *Angew. Chem. Int. Edit.* **45**, 4597-4601 (2006).

13. Roiter, Y. et al. *Langmuir* **25**, 6287-6299 (2009).

14. Middleton, E.R. & Rhoades, E. *Biophys. J.* **99**, 2279-2288 (2010).

15. Garrenton, L.S., Young, S.L. & Thorner, J. *Gene. Dev.* **20**, 1946-1958 (2006).

16. Zhao, C., Du, G.W., Skowronek, K., Frohman, M.A. & Bar-Sagi, D. *Nat. Cell. Biol.* **9**, 706-U171 (2007).

17. Fievet, F., Lagier, J.P., Blin, B., Beaudoin, B. & Figlarz, M. *Solid State Ionics* **32-33**, 198-205 (1989).

18. Sun, Y.G. & Xia, Y.N. *Science* **298**, 2176-2179 (2002).

19. Stober, W., Fink, A. & Bohn, E. *J. Colloid Interface Sci.* **26**, 62-& (1968).

20. Sioss, J.A., Stoermer, R.L., Sha, M.Y. & Keating, C.D. *Langmuir* **23**, 11334-11341 (2007).

21. Willets, K.A. & Van Duyne, R.P. *Annu. Rev. Phys. Chem.* **58**, 267-297 (2007).

22. Sherry, L.J. et al. *Nano Lett.* **5**, 2034-2038 (2005).

23. Mayer, K.M. & Hafner, J.H. *Chem. Rev.* **111**, 3828-3857 (2011).

24. Forstner, M.B., Yee, C.K., Parikh, A.N. & Groves, J.T. *J. Am. Chem. Soc.* **128**, 15221-15227 (2006).

25. Bacia, K. & Schwille, P. *Nat. Protoc.* **2**, 2842-2856 (2007).

26. Chen, Y., Muller, J.D., Eid, J.S. & Gratton, E. in *In New Trends in Fluorescence Spectroscopy: Applications to Chemical and Life Sciences*. (eds. Valeur, B. & Brochon, J.C.) 277-302 (Springer, Berlin, 2001).

27. Palik, E.D. *Handbook of Optical Constants of Solids*. (Elsevier, Amsterdam, 1998).

Fig. 1

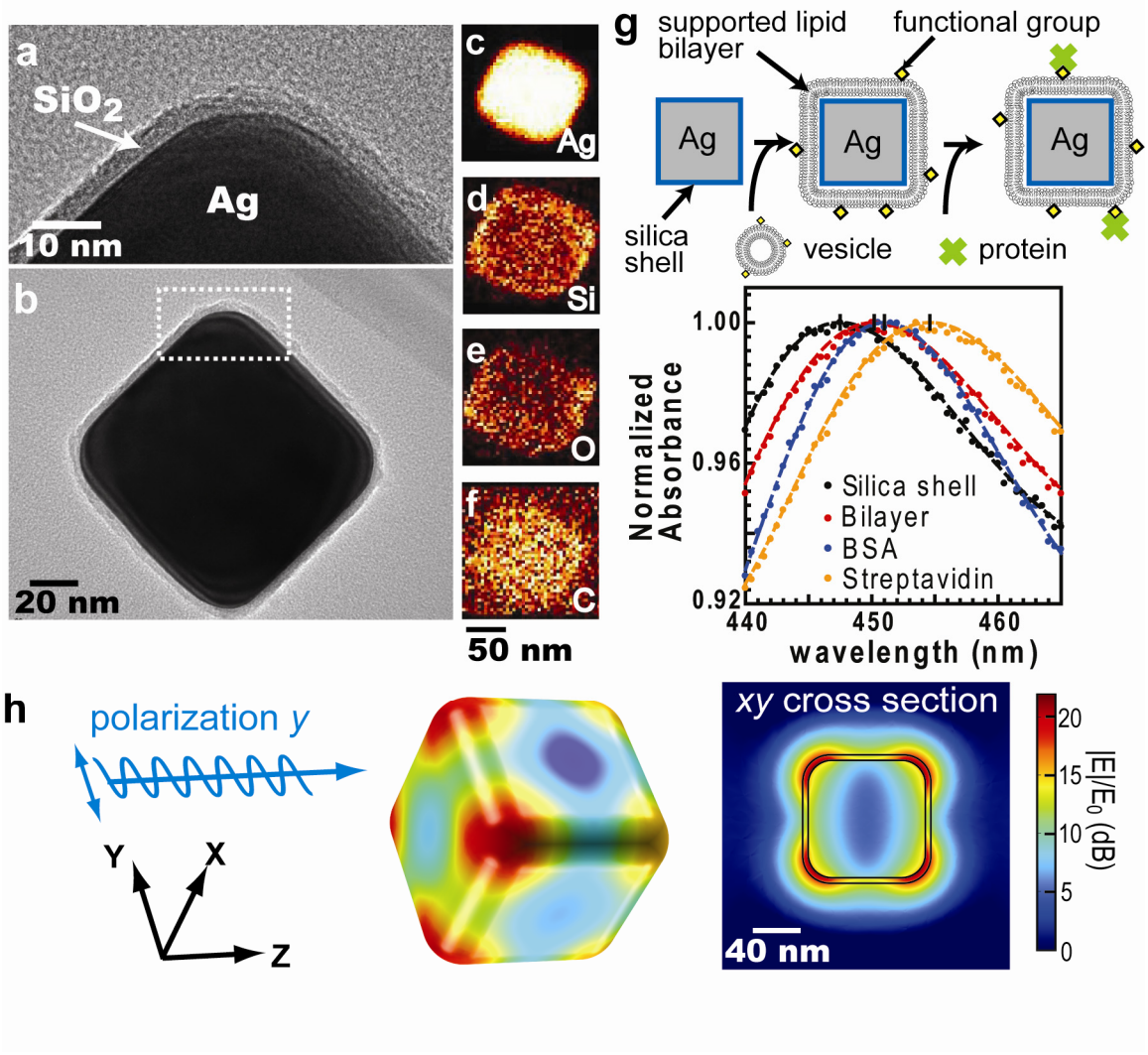
a
SiO2
Ag
10 nm
b
20 nm
c
Ag
d
Si
e
O
f
C
50 nm
g
supported lipid bilayer
functional group
Ag
Ag
Ag
silica shell
vesicle
protein
Normalized Absorbance
1.00
0.96
0.92
440
450
460
wavelength (nm)
Silica shell
Bilayer
BSA
Streptavidin
h
polarization y
Y
X
Z
xy cross section
40 nm
|E|/E0 (dB)
20
15
10
5
0

Fig. 2

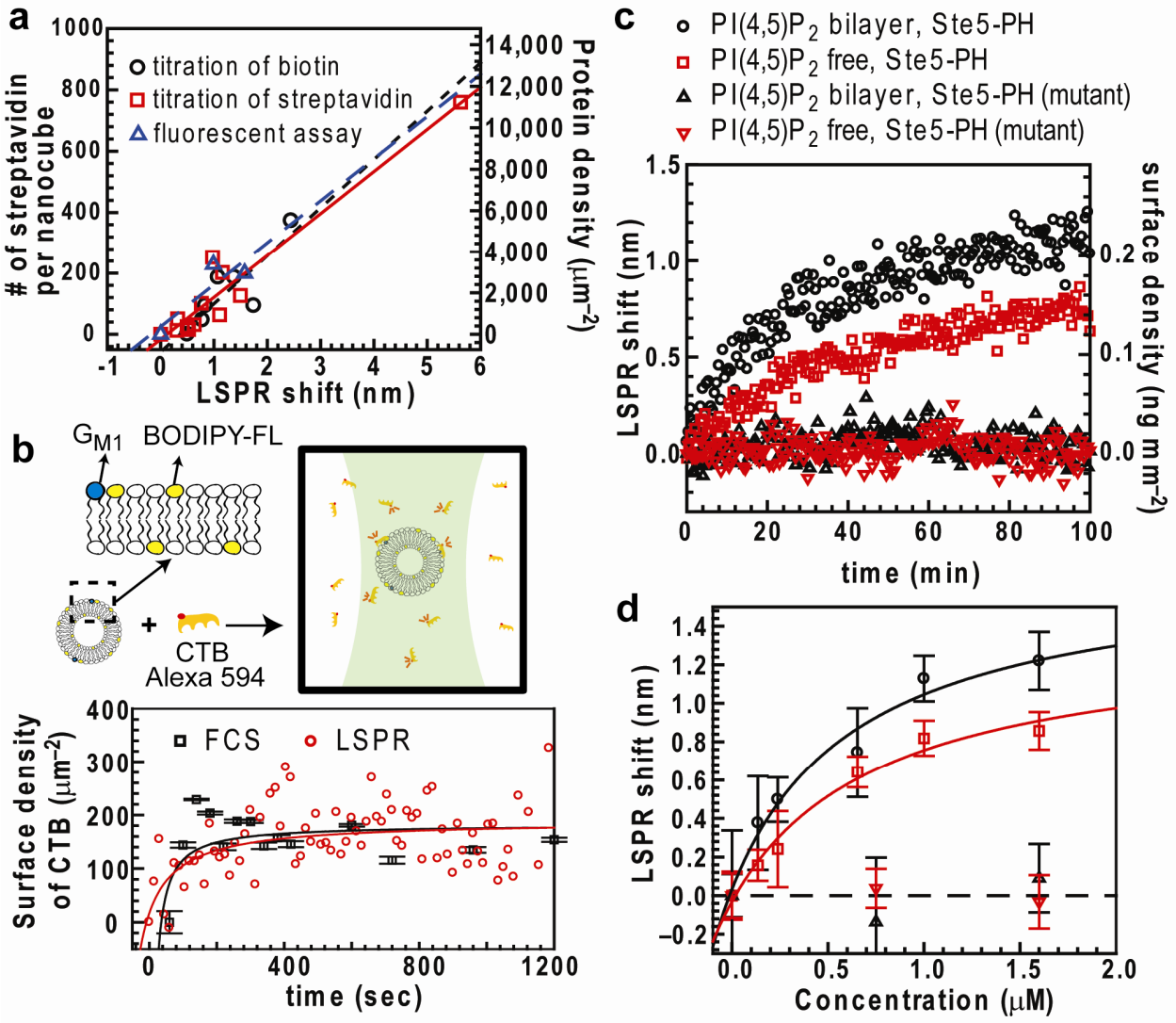
a
titration of biotin
titration of streptavidin
fluorescent assay
# of streptavidin per nanocube
Protein density (μm⁻²)
LSPR shift (nm)
b
G_M1
BODIPY-FL
CTB
Alexa 594
FCS
LSPR
Surface density of CTB (μm⁻²)
time (sec)
c
PI(4,5)P2 bilayer, Ste5-PH
PI(4,5)P2 free, Ste5-PH
PI(4,5)P2 bilayer, Ste5-PH (mutant)
PI(4,5)P2 free, Ste5-PH (mutant)
LSPR shift (nm)
surface density (ng mm⁻²)
time (min)
d
LSPR shift (nm)
Concentration (μM)

Supplementary information for:

Membrane-Protein Binding Measured with Solution-Phase Plasmonic Nanocube Sensors

Contents

- *Supplementary Figure:*
  - Figure 1: Scanning electron microscope (SEM) image of silver nanocube
  - Figure 2: Energy-dispersive X-ray spectroscopy (EDS) spectra of Ag@SiO_2 nanocube
  - Figure 3: Dark field light scattering of nanocube in different refractive index media
  - Figure 4: The light scattering spectra of nanocube detected at fixed angle in different refractive index media
  - Figure 5: Electromagnetic field enhancement profile along the nanocube diagonal computed in FEA
  - Figure 6: Normalized fluorescence recovery of supported lipid bilayers over three different substrates
  - Figure 7: The kinetics of streptavidin binding to biotinylated lipid at different concentrations monitored by nanocube sensors
  - Figure 8: The LSPR shift of Ag and Ag@SiO2 nanocubes in various refractive index media
  - Figure 9: The correlation between maximum absorbance of quadrupolar peaks and nanocube concentration
  - Figure 10: Estimated error of LSPR measurement
  - Figure 11: CTB binding measurements using FCS and nanocube assay
- *Supplementary Table:*
  - Table 1: The summary of protein surface density per LSPR peak shift
- *Supplementary discussion:*
  - Calibration of nanocube concentration & error of LSPR measurement
  - Calibration of LSPR shifts vs. protein density
  - Direct comparison of multi-component fluorescent correlation spectroscopy & nanocube detection
  - Detergent effects

Supplementary Figure 1

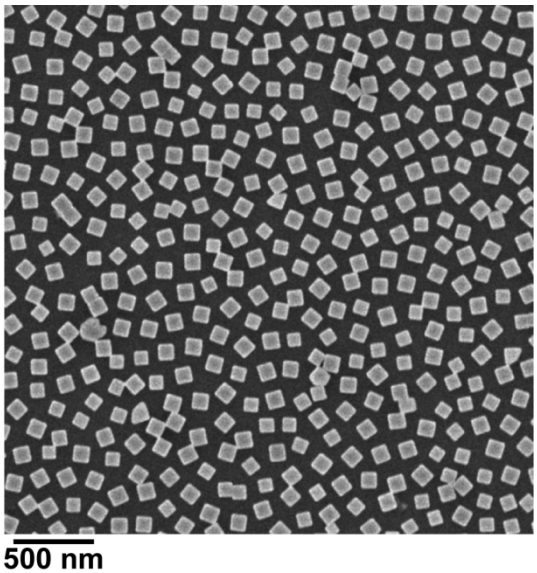

Figure S1. Scanning electron microscope (SEM) image of silver nanocube. Highly monodisperse nanocubes were synthesized using the polyol method.

Supplementary Figure 2

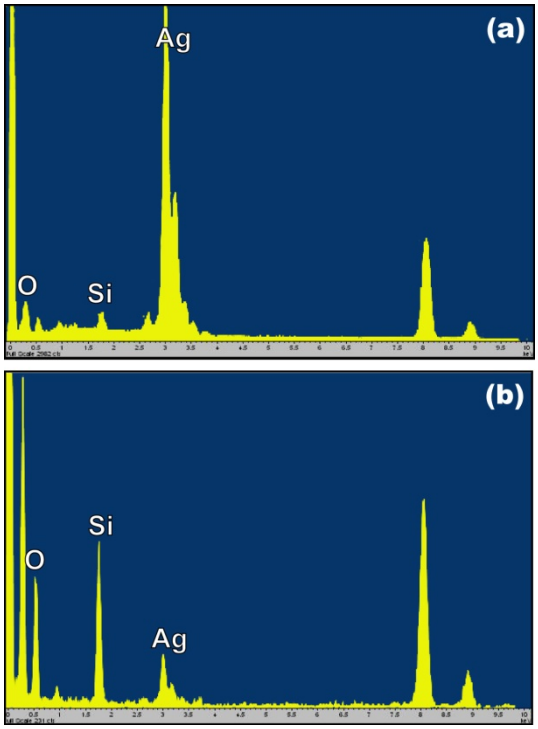

Figure S2. Energy-dispersive X-ray spectroscopy (EDS) spectra of Ag@SiO_2 nanocube. (a) EDS spectrum on the center of Ag@SiO_2 nanocube. (b) EDS spectrum on the silica shell of Ag@SiO_2 nanocube

Supplementary Figure 3

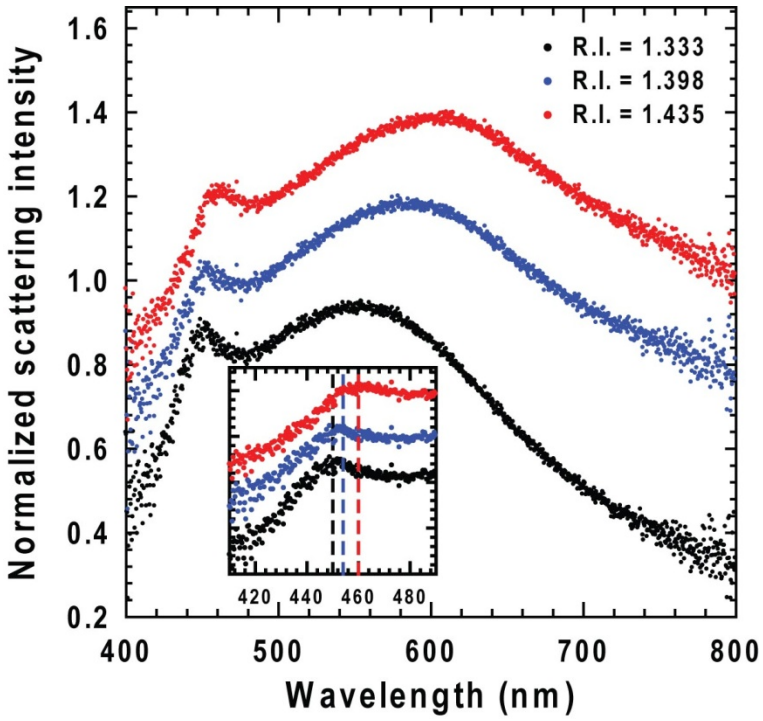

Figure S3. Dark field light scattering of nanocube in different refractive index (R.I.) media (water / glycerol solution). The spectra were detected with an inverted microscope coupled to a spectrometer. The inset shows the resolved details of quadrupolar peak. The dashed lines represent the position of maximum peak.

Supplementary Figure 4

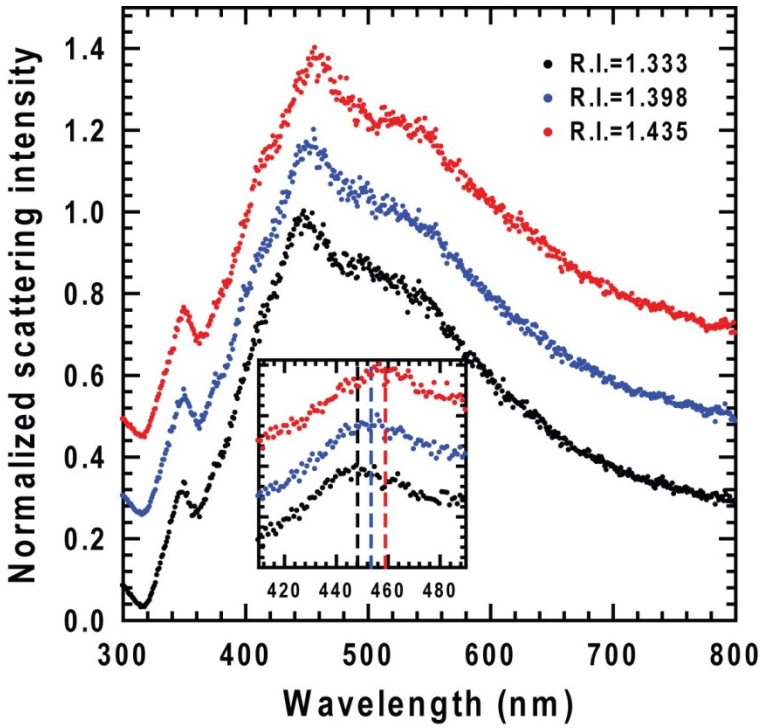

Figure S4. The light scattering spectra detected at a fixed angle (90 degree) in different refractive index (R.I.) media (water/glycerol solution) in a standard fluorescence spectrophotometer. The inset shows the resolved details of the quadrupolar peak. The dashed lines represent the position of the maximum peak.

Supplementary Figure 5

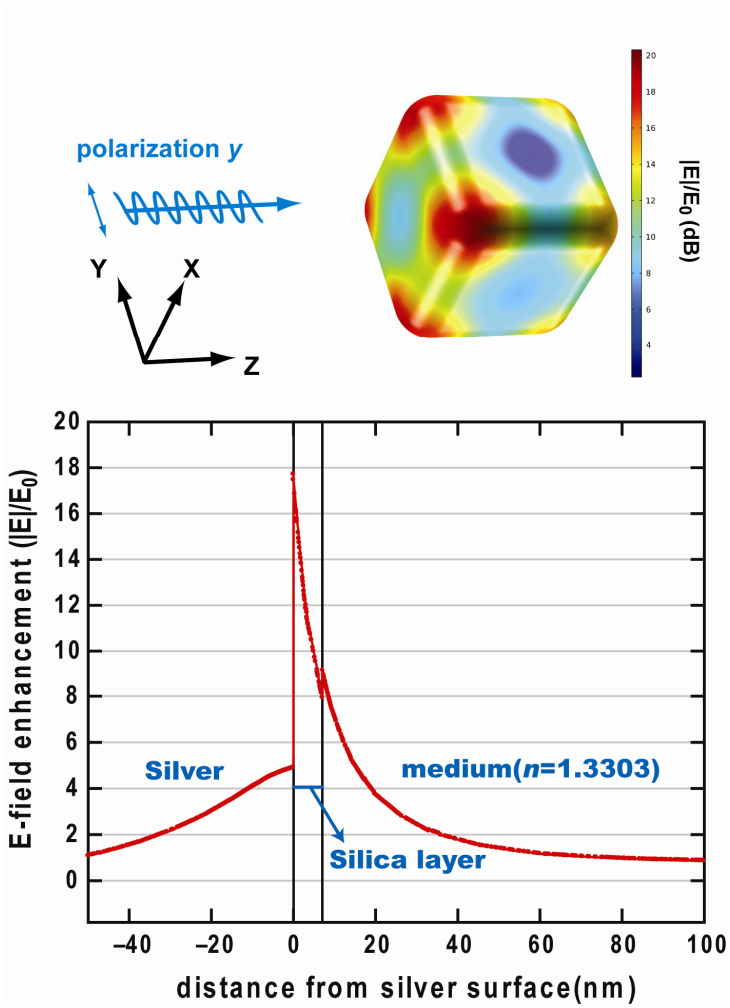

Figure S5. Electromagnetic field enhancement profile along the nanocube diagonal computed in FEA. The cross-section originates from the nanocube's center through a corner along the vector $(x,y,z) = (1,1,-1)$ in Fig. 1h. The model geometry of the silver nanocube was calculated from TEM, revealing a nanocube lateral dimension of 98 nm, 19 nm radius of curvature at the edges. The geometry of the silica shell was directly scaled up from silver nanocube to reach 4.0 nm shell thickness on facet, and thus the shell thickness through the corner is 7.0 nm in this cross-section.

Supplementary Figure 6

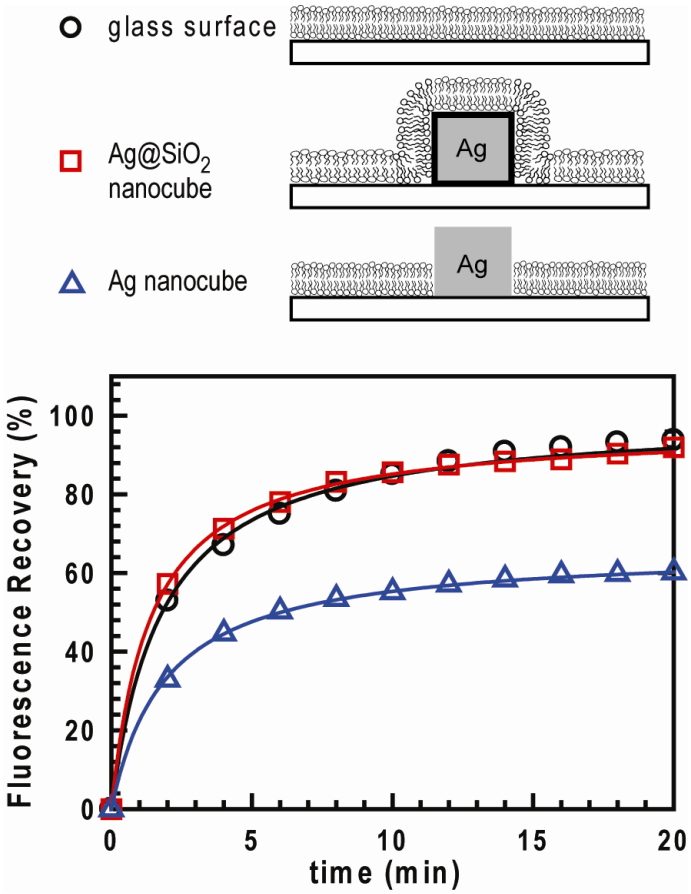

Figure S6. Normalized fluorescence recovery of supported lipid bilayers over three different substrates: (1) a bare glass surface, (2) Ag@SiO_2 nanocube adhered on a glass surface, and (3) Ag nanocube adhered on a glass surface. Nanocube-adhered substrates were prepared by drying a solution of nanocubes onto glass ($2 \cdot 10^8$ nanocubes on 18mm circle microscope cover glass). The two surfaces are expected to have similar nanocube densities after immobilization. No difference in recovery was observed between glass and Ag@SiO_2 nanocube substrates, although a higher immobile fraction was observed on the Ag nanocube substrate. Illustrations are not drawn to scale.

Supplementary Figure 7

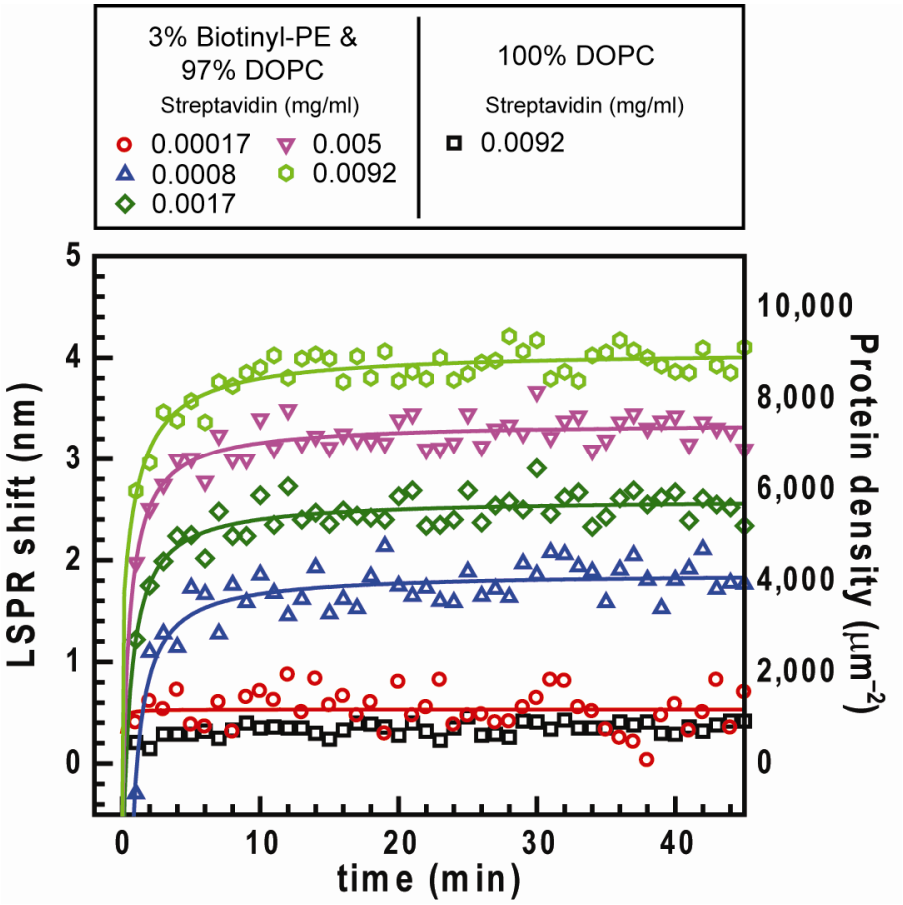

Figure S7. The kinetics of streptavidin binding to biotinylated lipid at different concentrations monitored by nanocube sensors. The biotinylated bilayer contains 3% biotinyl-cap-PE and 97% DOPC. The control bilayer is 100% DOPC. Fifteen consecutive LSPR spectra were collected to obtain an average baseline prior to kinetics measurements. Higher concentrations of streptavidin result in stronger shifts in the LSPR spectra. Streptavidin does not bind in the negative control bilayer (100% DOPC) and expectedly shows no LSPR shift.

Supplementary Figure 8

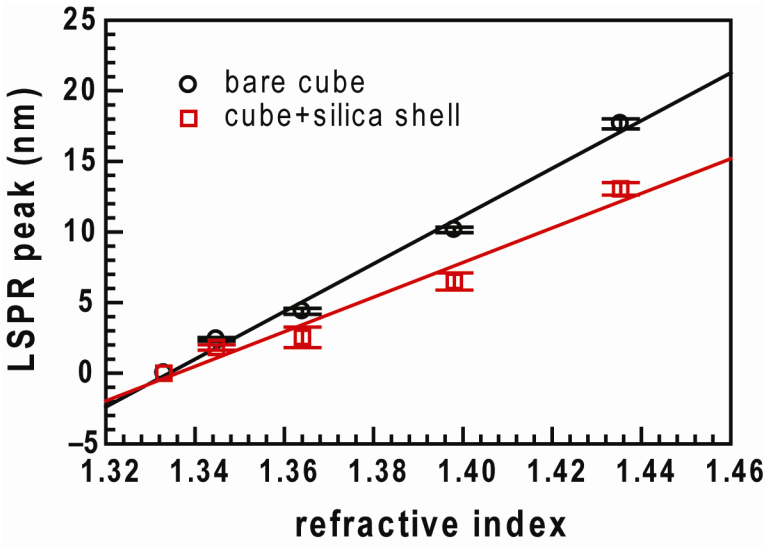

Figure S8. The LSPR shift of Ag and Ag@SiO_2 nanocubes in various refractive index media (water / glycerol solution). The averages and standard deviations of 3 different synthesis batches are presented. Ag@SiO_2 nanocubes show less sensitivity to refractive index change of media. The Ag nanocubes had a shift of 169 nm / RIU whereas the Ag@SiO_2 nanocubes had a shift of 123 nm / RIU.

Supplementary Figure 9

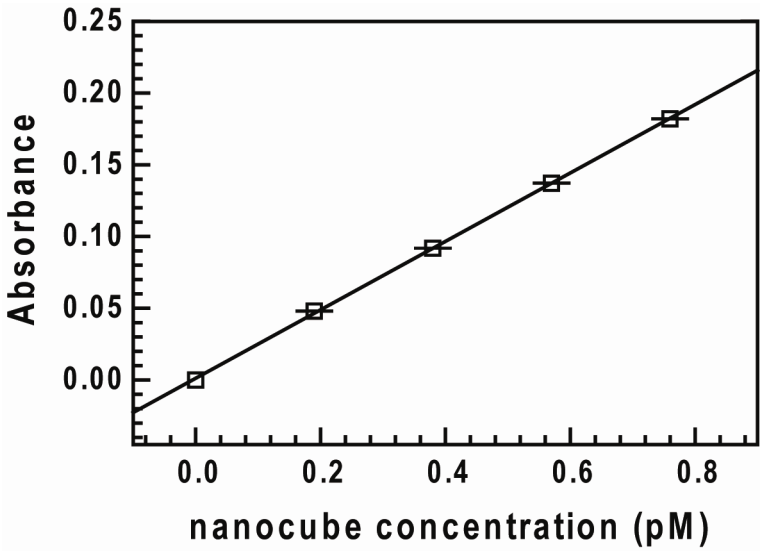

Figure S9. The correlation between maximum absorbance of quadrupolar peaks and nanocube concentration. Nanocubes deposited onto sedimentation chambers were directly imaged by dark field scattering microscopy. The linear relation between particle concentration and absorbance provides an approach to easily determine the nanocube concentration during the binding measurement[1]. (n=20, mean ± s.d.)

Supplementary Figure 10

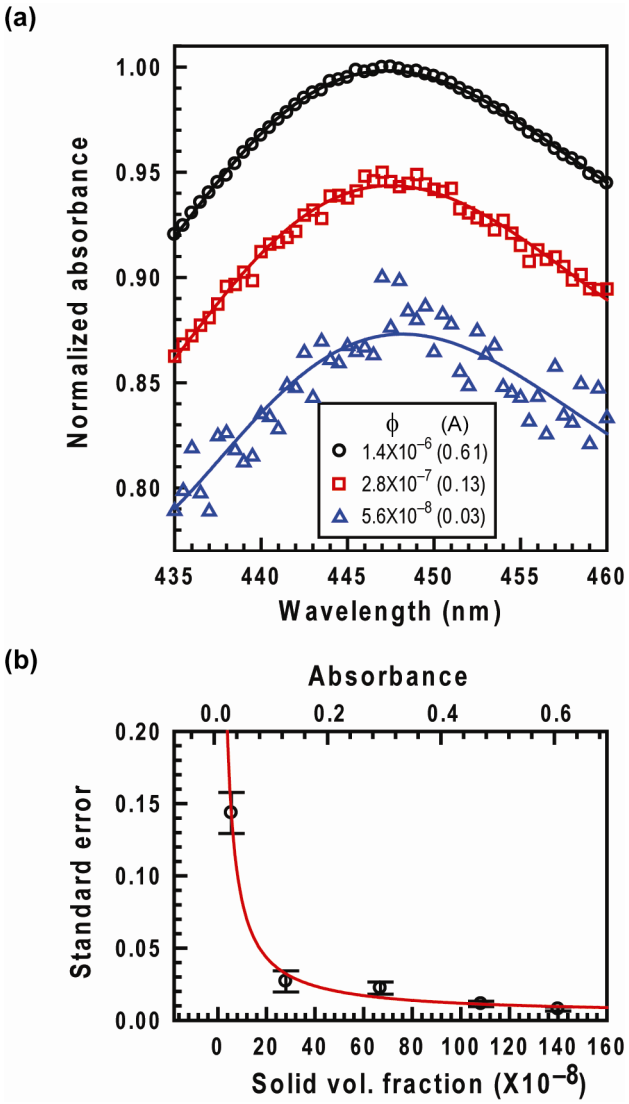

Figure S10. Estimated error of LSPR measurement. (a) LSPR spectra with various nanocube concentrations. The symbols and solid lines represent the raw data and the polynomial fits at different nanocube concentrations (solid volume fraction ϕ and maximum absorbance A). Lower concentrations of nanocubes show a lower signal-to-noise ratio and result in larger deviations of polynomial fits. (b) The standard error of 20 continuous measurements at different nanocube concentrations. (n=3, mean ± s.d.)

Supplementary Figure 11

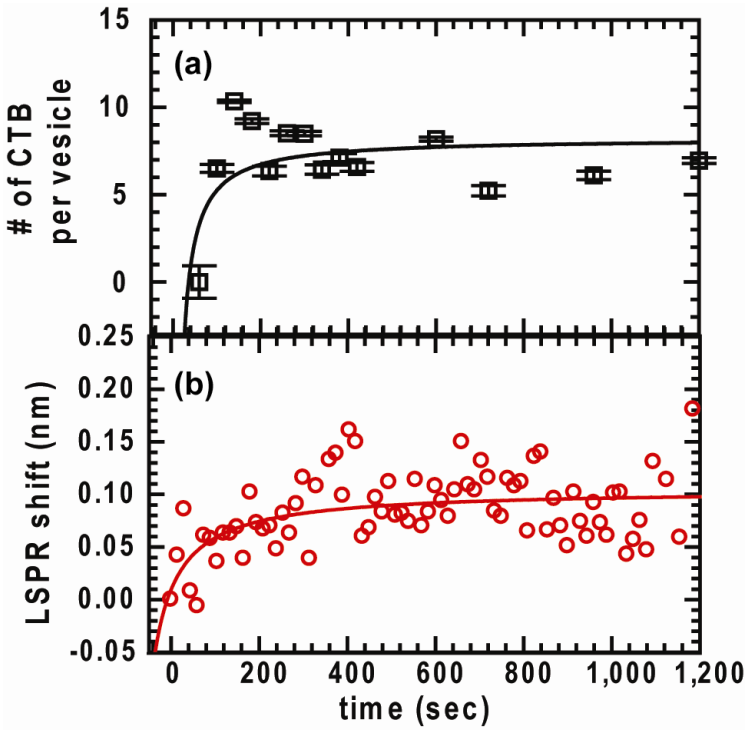

Figure S11. CTB binding measurements using FCS and nanocube assay. (a) The kinetics of Alexa 594-CTB binding to vesicles containing G_{M1} lipid monitored by multi-component FCS. (n=20, mean ± s.d.) (b) The kinetics of Alexa 594-CTB binding to supported lipid bilayer on Ag@SiO_2 nanocubes.

Supplementary Table 1

The summary of protein surface density per LSPR peak shift. The protein densities per LSPR shift measured by streptavidin titration, biotinyl-cap-PE titration, and fluorescence assay were evaluated from the slopes in Fig.2a. The value measured by FCS is calculated from the average LSPR shift after 1000 sec in Fig.2b. The average response determined by biotin-streptavidin system was 0.191 ng mm^{-2} nm^{-1}, consistent with the FCS measurements. Error limits are derived from the statistical error of curve fitting.

	# of protein / nanocube /LSPR shift (nm^{-1})	protein number density/ LSPR shift (μm^{-2} nm^{-1})	protein mass density/ LSPR shift (ng mm^{-2} nm^{-1})
		Streptavidin-biotin system	
Streptavidin titration	138±12	2033±180	0.178±0.016
biotin titration	135±37	1996±57	0.175±0.048
fluorescence assay	170±23	2512±352	0.220±0.031
		Average :	0.191±0.025
		CTB-G_{M1} system	
FCS	141±16	2084±234	0.191±0.021

Supplementary Discussion

Calibration of nanocube concentration and error of LSPR measurement

Determination of nanocube concentration in solution is necessary to evaluate the membrane surface area for kinetics calculations. To address this, nanocubes deposited onto sedimentation chambers were directly imaged by dark field scattering microscopy. A homemade image analysis program was developed to count the number of nanocubes in each imaging area. In addition, the nanocube concentration can be simply determined by measuring the absorbance using a UV-vis spectrophotometer (Supplementary Fig.9). The linear relation between particle concentration and absorbance was then used to determine the nanocube concentration during the binding measurement[1].

The prominent quadrupolar LSPR peak λ_{max} was interpolated by a polynomial fit. The higher concentration sample predictably provided a higher signal-to-noise ratio and hence higher precision of λ_{max} (Supplementary Fig.10a). The relation between precision of λ_{max} and nanocube concentration is shown in Supplementary Fig.10b. To obtain 0.01 nm precision of $\lambda_{max,}$ working concentration of nanocube measurement is at absorbance larger than 0.4. For 10 mm optical pathlength of spectrometer cells, 0.4 absorbance corresponds to the solid volume fraction 10^{-6} (Supplementary Fig.10b).

This solution-based sensing platform allows the analysis of ensembles in excess of 10^{12} nanocubes. In contrast to conventional LSPR assays, taking large ensemble measurements in solution reduces inaccuracies in the LSPR response caused by particle and bilayer variations thus increasing sensitivity and overall confidence in the measurement. Our calibration results provide the optimal working concentrations for the nanocube measurements. The high absorption of the nanocube sample, along with the narrow LSPR peak, results in highly precise interpolation of tiny shifts in λ_{max}. For the Ag@SiO_2 nanocube covered with 100% DOPC bilayer, the best resolution of LSPR measurements with a current UV-vis spectrophotometer is 0.01nm standard error of 20 consecutive scans (standard deviation=0.04 nm). It is correspondent to a protein density change of ~$1.9\cdot10^{-9}$ ng / μm^2. This indicates that the ideal sensitivity of the nanocube measurement can reach ~22 proteins /. μm^2 or 1.2 proteins per nanocube for a 53k Da size protein. The influences of protein binding may further introduce intrinsic fluctuation of signal. For example, the standard deviation of 20 measurements in Ste5 mutant system is 0.04 nm and standard error is 0.0l nm that is closed to ideal sensitivity. For Ste5 wildtype, the standard deviation and error is 0.065 nm and 0.015 nm that is a little bit higher. (Fig.2c)

Calibration of LSPR shifts vs. protein density

To further calibrate the correlation between LSPR shift and protein surface density on the membrane, three different approaches, (1) titrating biotinyl-cap-PE in bilayer, (2) titrating streptavidins in solution, and (3) measuring unbound fluorescent streptavidins, were employed here. The first approach is to alter the mole fractions of biotinyl-cap-PE in bilayer (0%, 0.025%, 0.05%, 0.1%, and 0.2 %). The bilayer coated Ag@SiO_2 nanocubes were incubated with excess streptavidin. By assuming a DOPC lipid footprint in supported bilayers of 0.72 nm^2, the average surface density of streptavidin was be calculated[2]. This approach varies the number of biotin binding sites on the membrane surface to calibrate the dependence of the LSPR shift on protein surface density.

The second approach is to change the protein density on the membrane surface by titrating the streptavidin concentration. A fixed number of small unilamellar vesicles (SUVs, 97% DOPC + 3% biotinyl-cap-PE) mixed with Ag@SiO_2 nanocubes were incubated with different amount of streptavidin. Because of the high affinity of biotin-streptavidin binding, we assume all streptavidin binds evenly and completely to vesicles and bilayers on Ag@SiO_2 nanocubes. The average streptavidin surface density on nanocubes can be evaluated by using a DOPC lipid footprint in supported bilayers.

In these two methods, we assume binding processes were complete after three hours incubation. Although previous a study shows the diffusion limitations of streptavidin binding to immobilized biotin are negligible[3], limited protein diffusion might erroneously lead to different calculated protein densities. Therefore, we introduce a third approach that measured unbound protein in the solution using streptavidin labeled with Alexa Fluo 647. In this approach, bilayer-coated Ag@SiO_2 nanocubes were incubated with different amount of fluorescent streptavidin for one hour. To separate bound from unbound streptavidin, streptavidin attached to bilayer-coated Ag@SiO_2 nanocubes was pulled down in a centrifuge. The concentration of unbound streptavidin remaining in the supernatant was determined by its fluorescence intensity in a spectrometer. Because nanocube concentration is known, the average streptavidin density on nanocubes was evaluated. To reduce the experimental error of fluorescent measurements, this approach required high nanocube concentrations to modulate the fluorescence intensity in supernatant.

Direct comparison of multi-component fluorescent correlation spectroscopy and nanocube detection

Fluorescence Correlation Spectroscopy (FCS) is a quantitative tool to locally measure molecular mobility and number densities of fluorescently labeled species[4]. In multi-components FCS measurements, we first determined the average number of vesicles and

CTB concentrations separately. Then, the same amount of vesicle and CTB were mixed to observe the kinetics of CTB binding.

The average number of vesicles N_v diffusing within the excitation spot was measured by FCS of vesicles doped with 0.5% BODIPY-FL-DHPE. These were performed with 488nm laser excitation at 0.2 mg / ml vesicle concentration. Twenty 120 sec measurements were taken and averaged to obtain statistical variations and fitted to an analytical expression of normal 3-D diffusion in a 3D-Gaussian volume for single diffusion species:

$$G(\tau) = \frac{1}{N} \frac{1}{1+\frac{\tau}{\tau_D}} \frac{1}{\sqrt{1+s^2 \frac{\tau}{\tau_D}}} \qquad \text{Eq (1)}$$

where N is the total number of diffusing particles, τ_D is the characteristic diffusion time, and s is a structure factor calibrated by a fluorescein standard. The average number of vesicles diffusing within the excitation spot N_v is equal to $1/G(0)$ from the analytical fitting result. With the same approach, the number of Alexa 594-CTB diffusing within the excitation spot, N_{CTB}, was measured under 568nm laser excitation. The concentration of Alex 594-CTB was 0.004 mg / ml. Finally, the same amount of Alexa 594-CTB (0.004 mg / ml) was mixed with vesicle solution (0.2mg / ml) to reach the same concentration as the previous separate measurements. Then, the time-resolved concentration was obtained by performing a 30 sec measurement every minute using 568 nm laser excitation. For each FCS curve, the value of $G(0)$ was extrapolated by fitting the curve to Eq. 1. Although Eq. 1 cannot fully describe multiple diffusing components with different brightnesses, it is sufficient to determine the value of $G(0)$.

The general expression for multicomponent 3-D diffusion is:

$$G(\tau) = \frac{1}{(\sum Q_k N_k)^2} \sum Q_j^2 N_j \frac{1}{1+\frac{\tau}{\tau_{Dj}}} \frac{1}{\sqrt{1+s^2 \frac{\tau}{\tau_{Dj}}}} \qquad \text{Eq(2)}$$

where Q_k is the average brightness for the component k. In this study, we simplified the system into two components, freely diffusing and vesicle-bound Alexa 594-CTB. We assumed the average number of Alexa 594-CTB binding to one vesicle was σ. Thus, the average brightness of the CTB component on one vesicle is σ times brighter than freely diffusing Alexa 594-CTB. It has been shown that a single Q can be used to accurately represent the average properties of the true distribution in this type of measurement [4, 5].

The $G(0)$ value of equation (2) can then be expressed as

$$G(0) = \frac{N_f + \sigma^2 N_v}{\left(N_f + \sigma N_v\right)^2} \qquad \text{eq(3)}$$

where σ is the number of bound CTB per vesicle, and N_f is the number of freely diffusing Alexa 594-CTB, which can be calculated from $N_f = N_{CTB} - \sigma N_V$. Using the measured N_v, N_{CTB}, and $G(0)$ values, the unknown σ can be computed from Eq (3). With the known average size of vesicles (120 nm), the surface density of CTB bound to vesicle can then be calculated (Supplementary Fig.11a).

For direct comparison, nanocube measurements were performed under the same experimental conditions as FCS. The same vesicle concentration used in FCS experiments was mixed with Ag@SiO_2 nanocubes to form supported lipid bilayers. Excess vesicles were not removed in order to maintain the same concentration of G_{M1} binding sites in the solution. The same amount of Alexa 594-CTB was added to the solution. Assuming that CTB binds equally to vesicles and bilayer-coated Ag@SiO_2 nanocubes, the surface density of bound CTB is the same on both surfaces. LSPR shifts were then monitored using a UV-Vis spectrophotometer (Supplementary Fig.11b). The LSPR shifts were converted to surface density using the LSPR response to protein mass change measured in the biotin-streptavidin system (0.191 ng mm^{-2} nm^{-1}, Supplementary Table 1). Kinetic binding curves measured by FCS and the nanocube assay reached equilibrium after 1000 sec (Supplementary Fig.11). The suitable working range for FCS depends on the size of the detection volume and the brightness of the fluorophores, and it typically falls below 100 nM [6]. Because concentration fluctuations from the ensemble average are crucial for FCS, these experiments were performed at a relatively low protein concentration and hence lower LSPR shift. Although the kinetic binding curves show a lower signal-to-noise ratio under such experimental conditions, the binding curves and final bound CBT density obtained from the two methods still show excellent agreement. In contrast to FCS, the detection of nanocube assay is not limited by analyte concentration because it measures the change of local refractive index. Practically, we have successfully performed protein binding measurement at concentration in the hundreds of micromolar range.

Detergent effect

During the measurement of Ste5-PH domain binding on supported phospholipid bilayers, we speculated that desorption of the lipid bilayer could influence the LSPR response. From our observations, adding detergent caused a blue shift that we attribute to disruptions of the bilayer. Detergents with low critical micelle concentration and high molecular weight are difficult to

remove by either dialysis or gel filtration[7]. Our results suggest that the use of detergent should be eliminated in all protein preparation steps for membrane protein binding measurements. In this paper, the use of detergent was therefore eliminated during protein purification to avoid these effects.

Reference

1. Haiss, W., Thanh, N.T.K., Aveyard, J. & Fernig, D.G. *Anal. Chem.* **79**, 4215-4221 (2007).

2. Vacklin, H.P., Tiberg, F. & Thomas, R.K. *Biochim. Biophys. Acta, Biomembr.* **1668**, 17-24 (2005).

3. Balgi, G., Leckband, D.E. & Nitsche, J.M. *Biophys. J.* **68**, 2251-2260 (1995).

4. Middleton, E.R. & Rhoades, E. *Biophys. J.* **99**, 2279-2288 (2010).

5. Pu, M.M., Fang, X.M., Redfield, A.G., Gershenson, A. & Roberts, M.F. *J. Biol. Chem.* **284**, 16099-16107 (2009).

6. Krichevsky, O. & Bonnet, G. *Rep. Prog. Phys.* **65**, 251-297 (2002).

7. Rigaud, J.L., Levy, D., Mosser, G. & Lambert, O. *Eur. Biophys. J.* **27**, 305-319 (1998).

DISCLAIMER

This document was prepared as an account of work sponsored by the United States Government. While this document is believed to contain correct information, neither the United States Government nor any agency thereof, nor the Regents of the University of California, nor any of their employees, makes any warranty, express or implied, or assumes any legal responsibility for the accuracy, completeness, or usefulness of any information, apparatus, product, or process disclosed, or represents that its use would not infringe privately owned rights. Reference herein to any specific commercial product, process, or service by its trade name, trademark, manufacturer, or otherwise, does not necessarily constitute or imply its endorsement, recommendation, or favoring by the United States Government or any agency thereof, or the Regents of the University of California. The views and opinions of authors expressed herein do not necessarily state or reflect those of the United States Government or any agency thereof or the Regents of the University of California.